International Journal of Theoretical Physics (2019) 58:2757–2769
https://doi.org/10.1007/s10773-019-04106-7

Enhanced Spin Seebeck Efficiency in Closed Triple Quantum Dots Ring with Spin-Dependent Interdot Couplings

Shu-Chao Yu[1,2] · Feng Chi[2] · Li-Ming Liu[2] · Hongwei Chen[1]

Received: 19 April 2018 / Accepted: 27 July 2018 / Published online: 31 July 2019

Abstract
Spin Seebeck effect (SSE) in triple quantum dots coupled to ferromagnetic leads is studied by using the Keldysh nonequilibrium Green's function technique. In low temperature regimes, the Fano effect arising from the interferences between the isolated states and the continuum plays an dominant role in the electronic and thermoelectric transport processes. The Seebeck coefficient depends on spin degree of freedom when the leads' magnetic moments are in parallel configuration. When the leads' polarization is varied, the charge Seebeck coefficients are less influenced, whereas those of the spin counterparts are obviously changed. The magnitudes of both the SSE coefficient and the spin figure of merit (FOM) will be enhanced by increasing the asymmetry of the leads' spin polarization. In the presence of the spin-dependent interdot couplings, the strengths of the charge and spin thermoelectric quantities are individually suppressed and enhanced, and then the magnitudes of the SSE coefficient and the spin FOM are comparable to those of the charge counterparts. Interestingly, by the joint effects of the ferromagnetism on the leads and the spin-dependent interdot couplings, the spin thermopower can even changes its sign around the antiresonance states.

Keywords Spin Seebeck effect · Quantum dots · Spin-dependent interdot coupling

1 Introduction

The old phenomenon of thermoelectricity, which converts heat into electricity or vice versa, has recently gained renewed attention in meso- and nano-scopic structures [1, 2]. This research subject is of fundamental interest for managing both the generated heat in nanoelectronic devices and the motion of elementary carriers in condensed matter physics. The thermoelectric energy-conversion efficiency in low-dimensional systems is remarkably enhanced by the typical δ-like density of states arising from the quantum confinement

✉ Feng Chi
chifeng@semi.ac.cn

[1] State Key Laboratory of Electronic Thin Films and Integrated Device, University of Electronic Science and Technology of China, Chengdu, 610054, China

[2] School of Electronic and Information Engineering, University of Electronic Science and Technology of China, Zhongshan Institute, Zhongshan, 528400, China

effect, the suppressed phonon thermal conductivity by the interface scattering, and the strong and adjustable Coulomb interaction. These unique properties lead to the violation of Wiedemann-Franz law [3, 4], according to which the value of $(\kappa_e + \kappa_{ph})/(G_c T)$ is constant in all systems, where $\kappa_{e(ph)}$ is the electron (phonon) thermal conductivity, G_c the charge conductance, and T the system equilibrium temperature. As a result of it, the thermoelectric efficiency characterized by the dimensionless figure of merit (FOM) $Z_c T = S_c^2 G_c T/(\kappa_e + \kappa_{ph})$ can hardly overcome 1, where S_c is the charge thermopower standing for the generated charge voltage by the temperature gradient applied across the system under open circuit condition.

More than three decades ago, a subject of spintronics emerged which focuses on the utilization of electron spin with the help of ferromagnetic materials and electrical spin control means, such as gate voltage and spin-orbit interactions [5, 6]. In fact, along with the development of this field, some investigations have been devoted to the interplay between heat and spin current, which leads to another filed of spin Seebeck effect (SSE) or spin-caloritronics, the spin version of the thermoelectric effect [7]. The most important issue in this field is the generation of a spin current (or bias) as a result of a temperature gradient, which was successfully demonstrated in experiments by Uchida and his coworkers in ferromagnetic metals [8], semiconductors [9], and conductors [10]. This effect can even be realized in magnetic insulators [11, 12] and provides the possibility of converting the heat energy in insulators into electrical one in adjacent conductors by inverting the generated spin current into a charge one. Such a process is beyond the reach of the conventional thermoelectric technologies. The SSE effect also possess some other unique features ideal for thermoelectric applications because the heating power applied to the system can easily change the accumulation of majority and minority spins. The sign of the SSE coefficient can also be switched by simply reversing the direction of the temperature gradient. The results enable many possible applications in designing energy saving spintronic devices with increased efficiency in terms of thermoelectric effect [13–17].

At the present stage, the efficiency of the SSE technology is still very small [18–24]. Many efforts have been made to enhance the spin signals including the spin thermopower S_s denoting the spin bias generated by the temperature gradient and the dimensionless spin FOM $Z_s T$ representing the SSE efficiency [7]. As a typical nanostructure, quantum dots (QDs) [25, 26] with discrete energy levels and tunable Coulomb interaction have been proposed as a good candidate for enhancing the SSE efficiency [27]. Various systems composed of QDs coupled to different types of leads, such as normal metallic [28–32], ferromagnetic [27, 33–38], superconductor or hybridized ones [39–42], were put forward in recent years. Many interesting results and applications were found. For example, when the QDs is coupled to ferromagnetic leads, both the magnitude and the signs of the thermopower can be adjusted by changing the configurations and the spin polarizations of the leads' magnetic moments, and the magnitude of the spin signals are comparable to those of the charge ones [33, 34, 38]. The SSE is also promising in detecting the Majorana states when the dots is coupled to topological superconductors [39]. In multi-QDs structures, Fano and Dick effects emerge due to the interference between the discrete state and the continuum [43]. These effects are characterized by the δ-like density of states and sharp change of the line-shapes of the electron conductance and thermal conductivity. It should be noted that the subtle Kondo effect will also have an impact on the electron and thermoelectric transport processes. But as compared to the previous two effects, its influences are relatively less distinct and then is neglected in the present paper. It has already been demonstrated that the SSE efficiencies are significantly enhanced in a T-shaped double QDs system and closed Aharonov-Bohm rings with spin-orbit interactions and ferromagnetic leads [28–32].

In the present paper, we study the SSE in a triple QDs system connected to ferromagnetic leads with spin-dependent interdot couplings (see Fig. 1). The system is modeled by a multi-impurities Anderson Hamiltonian [28, 44–46]. We calculate the electron transmission probability with the help of the equation of motion method in the framework of nonequilibrium Keldysh Green's functions technique. We show that the spin thermopower and the spin FOM are tunable by changing the asymmetry of the three QDs' levels, the ferromagnetism on the leads, and the strength of the spin-dependent interdot couplings, which can be realized by applying a static magnetic field on the tunneling junction between two QDs, making the electron spin perform Larmor precession when it passes through the potential barrier [47, 48]. Generating spin current based on spin-dependent interdot couplings has been discussed in some previous works [50, 51], but its possible influence on the thermoelectric transport has not been studied yet.

2 Model

The Hamiltonian of the triple QDs interferometer can be written as $H = H_{leads} + H_{dots} + H_{dots-leads}$, where the first term on the right side is as follows [28, 44],

$$H_{leads} = \sum_{k\beta\sigma} \varepsilon_{k\beta\sigma} c^{\dagger}_{k\beta\sigma} c_{k\beta\sigma}, \tag{1}$$

where $c^{\dagger}_{k\beta\sigma}$ ($c_{k\beta\sigma}$) creates (annihilates) an electron with momentum k, spin index σ ($\sigma =\uparrow,\downarrow$), and energy $\varepsilon_{k\beta\sigma}$ in the β-th ($\beta = L,R$) lead.

$$\begin{aligned} H_{dots} = & \sum_{i\sigma} \left[\varepsilon_i d^{\dagger}_{i\sigma} d_{i\sigma} + \frac{U_i}{2} d^{\dagger}_{i\sigma} d_{i\sigma} d^{\dagger}_{i\bar{\sigma}} d_{i\bar{\sigma}} \right] \\ & + \sum_{\sigma} \left(t_{12,\sigma} d^{\dagger}_{1\sigma} d_{2\sigma} + t_{23,\sigma} d^{\dagger}_{2\sigma} d_{3\sigma} + t_{31,\sigma} d^{\dagger}_{3\sigma} d_{1\sigma} + H.c \right), \end{aligned} \tag{2}$$

where $d^{\dagger}_{i\sigma}$ ($d_{i\sigma}$, $i = 1,2$) is the creation (annihilation) operator for an electron in dot i with spin σ and energy ε_i. U_i is the intradot Coulomb interaction in dot i, and $t_{ij,\sigma}$ the spin-dependent interdot coupling.

$$H_{dots-leads} = \sum_{k,\sigma} (V_{kL\sigma} c^{\dagger}_{kL\sigma} d_{1\sigma} + V_{kR\sigma} c^{\dagger}_{kR\sigma} d_{2\sigma} + H.c), \tag{3}$$

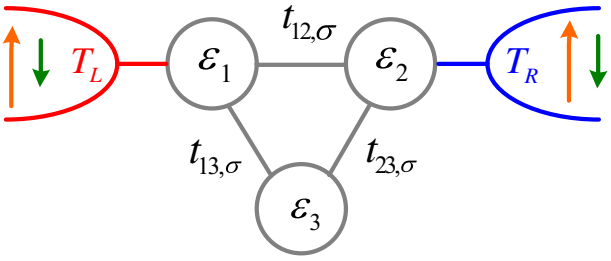

Fig. 1 Schematic plot of the triple quantum dots connected to the left and right ferromagnetic lead that are held at temperatures of T_L and T_R, respectively. The magnetic moments of the two leads are in parallel configuration, and the majority and minority spins are individually spin-up and spin-down. Each dot i having energy level of ε_i is tunnel coupled to the other two with spin-dependent strengths of $t_{ij,\sigma}$

in which $V_{k\beta\sigma}$ describes the spin-dependent dot-lead tunnel matrix element in the presence of ferromagnetic leads.

In the linear response regime, i.e., under infinitely small bias voltage ΔV and temperature gradient ΔT between the two leads, the spin-resolved electric and heat currents through the system can be individually written as [33–35]

$$J_{e,\sigma} = -e^2 K_{0,\sigma}\Delta V + \frac{e}{T}K_{1,\sigma}\Delta T, \tag{4}$$

$$J_{h,\sigma} = eK_{1,\sigma}\Delta V - \frac{1}{T}K_{2,\sigma}\Delta T, \tag{5}$$

where e is the electron charge and T the system equilibrium temperature. The coefficients $K_{n,\sigma}$ in the above equation are given by [33–35]

$$K_{n,\sigma} = \frac{1}{\hbar}\int (\varepsilon-\mu)^n \left[-\frac{\partial f(\varepsilon,\mu)}{\partial\varepsilon}\right] T_\sigma(\varepsilon)\frac{d\varepsilon}{2\pi}, \tag{6}$$

where $\hbar$ is the reduced Planck's constant, $\mu = \mu_L = \mu_R$ the leads' chemical potential, $f(\varepsilon,\mu) = 1/\{1 + \exp[(\varepsilon - \mu)/k_BT]\}$ the Fermi distribution function with Boltzmann constant k_B.

In (6), the transmission coefficient $T_\sigma(\varepsilon)$ for each spin component can be obtained in terms of the Green's function as [33, 34] $T_\sigma(\varepsilon) = G^a_{12,\sigma}(\varepsilon)\Gamma^R_\sigma G^r_{21,\sigma}(\varepsilon)\Gamma^L_\sigma$, in which $G^{r(a)}_{ij,\sigma}$ is the element of the Keldysh retarded (advanced) Green's function $\mathbf{G}^{r(a)}_\sigma(\varepsilon)$ in a 3×3 matrix form. In the presence of Coulomb interaction, the Green's functions can not be exactly solved, one has to make approximations. Here we adopt the same truncation method for the higher-order Green's function as in Refs. [52,53], in which the free dot Green's functions $\mathbf{g}^r_\sigma(\varepsilon)$ are first exactly calculated. The couplings between the dot and leads are then included as the self-energies $\mathbf{\Sigma}^r_\sigma$. The obtained Green's function can be written in Dyson equation form of $\mathbf{G}^r_\sigma(\varepsilon) = \left[\mathbf{g}^{r-1}_\sigma(\varepsilon) - \mathbf{\Sigma}^r_\sigma\right]^{-1}$, where the 3×3 matrix $\mathbf{g}^r_\sigma(\varepsilon)$ is the free Green's function of the dots, i.e., when the dots are free from interaction between the leads and interdot couplings. Its diagonal elements are

$$g^r_{ii,\sigma} = \frac{\varepsilon - \varepsilon_i - U_i(1-n_{i\bar{\sigma}})}{(\varepsilon-\varepsilon_i)(\varepsilon-\varepsilon_i-U_i)}, \tag{7}$$

where the dot occupation number needs to be self-consistently calculated from the equation of $n_{i\sigma} = -(1/\pi)\int f(\varepsilon,\mu)\mathrm{Im}G^r_{ii,\sigma}(\varepsilon)d\varepsilon$. The off-diagonal elements of $\mathbf{g}^r_\sigma(\varepsilon)$ are all zero. The spin-dependent line-width function $\Gamma^{L/R}_\sigma$ is written as $\Gamma^{L/R}_\sigma = \Gamma^\beta_0(1 + p_\beta)$, in which p_β stands for the leads' spin polarization, and $\Gamma^{L/R}_0 = \left(\Gamma^{L/R}_\uparrow + \Gamma^{L/r}_\downarrow\right)/2$ [33–35]. The retarded self-energy $\mathbf{\Sigma}^r_\sigma$ is also a 3×3 matrix,

$$\mathbf{\Sigma}^r_\sigma = \begin{bmatrix} -i\Gamma^L_\sigma/2 & t_{12,\sigma} & t_{13,\sigma} \\ t^*_{12,\sigma} & -i\Gamma^R_\sigma/2 & t_{23,\sigma} \\ t^*_{13,\sigma} & t^*_{23,\sigma} & 0 \end{bmatrix}. \tag{8}$$

The thermopower (Seebeck coefficient) of each spin component S_σ is calculated under the condition of vanishing charge current $J_e = J_{e,\uparrow} + J_{e,\downarrow} = 0$, and is given by [33–35] $S_\sigma = -K_{1,\sigma}/(eTK_{0,\sigma})$, and the charge (spin) thermopower is given by $S_{c(s)} = S_\uparrow + (-)S_\downarrow$. The charge (spin) FOM is $Z_{c(s)}T = S^2_{c(s)}G_{c(s)}T/(\kappa_e + \kappa_{ph})$, in which the charge (spin) conductance $G_{c(s)} = G_\uparrow + (-)G_\downarrow$ with $G_\sigma = e^2K_{0,\sigma}$. The electric thermal conductivity is

$$\kappa_e = \frac{1}{T}\sum_\sigma\left(K_{2,\sigma} - \frac{K^2_{1,\sigma}}{K_{0,\sigma}}\right). \tag{9}$$

In the present paper, we set $\kappa_{ph} = 0$ since the phonon transport can be blockaded by particular device design. In some works, the phonon conductivity is set to be $(\pi^2 k_B^2)/(3hT)$ [27], which does not change the qualitative results in the present paper.

3 Numerical Results and Discussions

In the following numerical calculations, we set $\Gamma_0^L = \Gamma_0^R = \Gamma_0 = 1$ as the energy unit, and fix the equilibrium chemical potential of the leads $\mu = 0$ as the energy zero point. The dot levels are set to be $\varepsilon_1 = \varepsilon_0$, and $\varepsilon_{2(3)} = \varepsilon_0 + (-)\Delta$, where Δ stands for the level detuning. We assume symmetric interdot couplings and set $t_{12,\sigma} = t_{23,\sigma} = t_{31,\sigma} = t_c + \sigma\delta t_c$.

Figure 2 presents the impact of the level detuning on the spin-dependent conductance in the absence of intradot Coulomb interaction ($U_i = 0$) and dependence of the interdot coupling on spin ($\delta t_c = 0$). As expected [45, 46], for the case of $\Delta = 0$ the conductance of each spin component $G_{\uparrow(\downarrow)}$ shows an antiresonance at $\varepsilon_0 = \mu = 0$ (see the solid lines) and two Lorentzian-like resonant peaks at $\varepsilon_0 = \mu \pm \sqrt{2t_c^2}$ [44]. Turning on the level detuning ($\Delta \neq 0$), the positions of the Fano antiresonances are shift to $\pm\Delta$, and the resonances emerge at $\varepsilon_0 = \mu$ and $\varepsilon_0 = \mu \pm \sqrt{\Delta^2 + 2t_c^2}$ [44]. The antiresonance in the conductance, which

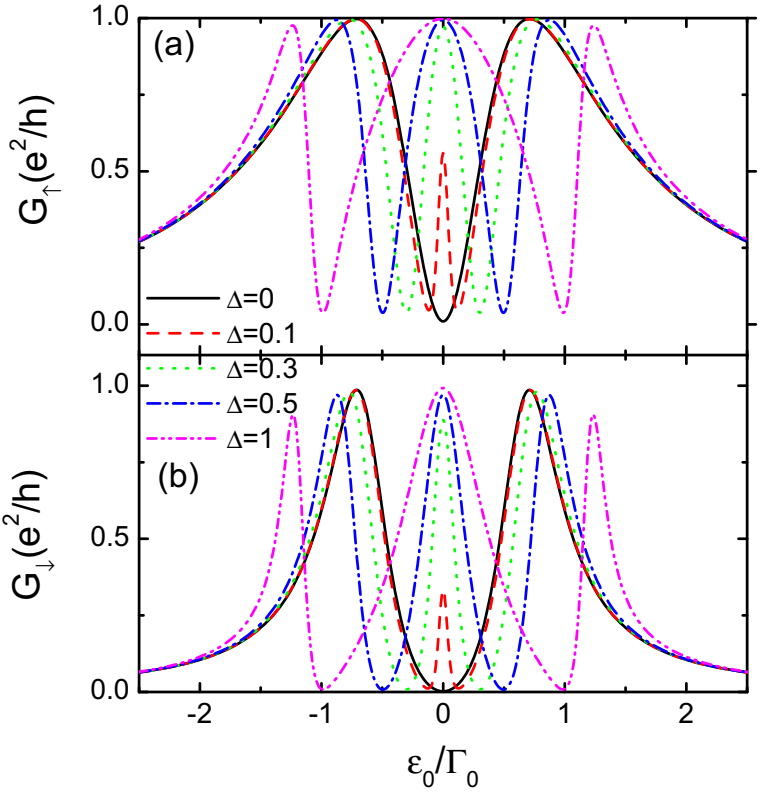

Fig. 2 Spin-dependent electrical conductance G_σ as functions of the dot level ε_0 for different values of the level shift Δ with $k_B T = 0.02\Gamma_0$. Other parameters are $t_c = 0.5\Gamma_0$, $\delta t = 0$, $p_L = p_R = 0.4$ and $U = 0$

induces large thermopower and FOM, originates from the quantum interference effect. For the present triple QDs ring, there are two different transport channels for the tunneling electrons, one is from the left lead to QD-1, to QD-2, and then to the right lead. The other channel is from the left lead to QD-1, to the side-coupled QD-3, and then to QD-2 and finally to the right lead. The tunneling electrons from the two paths will acquire different phases. When they meet in the QDs, the destructive (constructive) interference effect leads to the antiresonance (resonance) in the conductance. In fact, the anti-resonant and resonant peaks also emerge in the electron thermal conductivity κ_e (not shown here). The width of conductance's peak of each spin component is determined by the corresponding line-width function $\Gamma_\sigma = \Gamma_\sigma^L + \Gamma_\sigma^R$. From Fig. 2a and b one can see that the peaks of the spin-up conductance $G_\uparrow$ is wider than that of the spin-down one $G_\downarrow$ for the parallel configuration considered here.

The charge thermopower S_c in Fig. 3a exhibits a sawtoothlike shape with respect to the dot level, which is consistent with the experimental observations and previous theoretical predictions [54, 55]. It develops two peaks with opposite signs at the two sides of each antiresonance in the conductance. The origin of the positive and negative peaks is as follows: Assuming the left and right leads are respectively in higher and lower temperature due the presence of a small temperature gradient. When the dot level ε_0 is higher than the anti-resonant state, the heat is mainly carried by electrons, in other words, more transmission spectral weight lies in the electron channel than in the hole one, resulting in positive value of thermopower. Oppositely, if the heat transport through the hole channels is predominant when ε_0 is lower than the anti-resonant state, and then the thermopower is negative. When the dot level is aligned to the anti-resonant channels, the thermopower vanishes because the same amount of electrons and holes are transporting in opposite directions and then the heat carried by them are self-consistently balanced. With increasing level detuning Δ, the

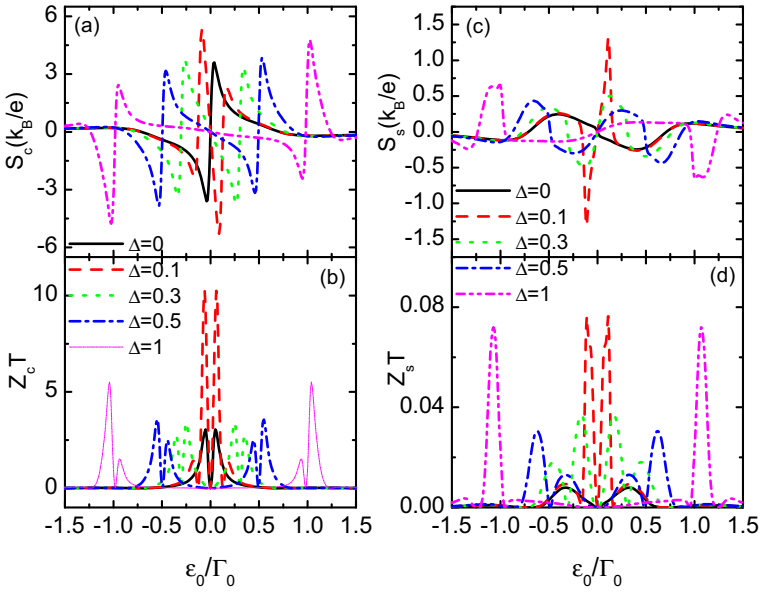

Fig. 3 **a** Charge Seebeck coefficient S_c, **b** charge figure of merit Z_cT, **c** spin Seebeck coefficient, and **d** spin figure of merit varying with the dot level ε_0 for different Δ. Parameters are as in Fig. 2

positions of the peaks in the thermopower are also shifted with changed magnitudes. As compared to Fig. 2, one can see that the optimized Z_cT value does not emerge at either the maximum conductance or the minimum conductance as illustrated in Fig. 3b. The largest value for Z_cT is obtained at the two sides of each anti-resonant state where the thermopwer has a peak value. Such a double peak configuration of the FOM is consistent with previous theoretical results. The line-shapes of the spin thermopower S_s and FOM Z_sT in Fig. 3c and d essentially resemble those of the charge counterparts, respectively. The peaks' width of the spin thermopower in Fig. 3c are much wider than those in Fig. 3a with smaller values. It indicates that usually the thermospin signals induced solely by the ferromagnetic leads are much weaker than the charge ones. It is shown that the value of Z_sT in Fig. 3(d) is about three orders smaller than that of Z_cT in Fig. 3b.

To find a optimized temperature for the thermoelectric efficiency, we present counter plots of Z_cT and Z_sT in Fig. 4 for fixed value of $\Delta = 0.3\Gamma_0$. It is seen that with increasing temperature, both Z_cT and Z_sT first increase and then decrease. Large Z_cT value in Fig. 4a is obtained around $0.2\Gamma_0 \sim 0.6\Gamma_0$, but the regime of the optimal temperature for Z_sT

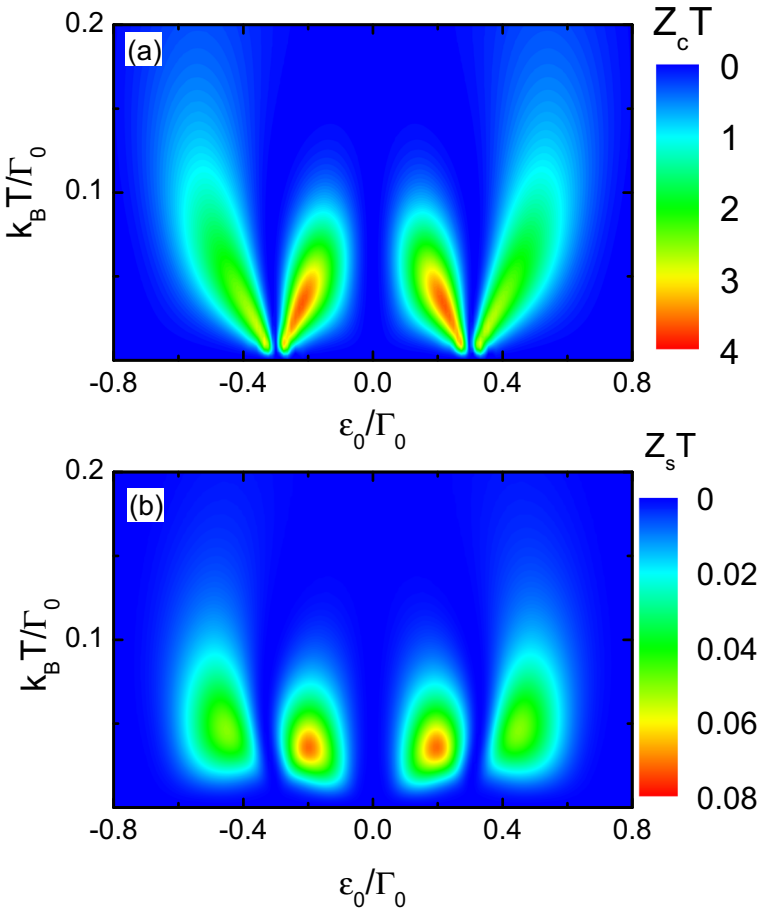

Fig. 4 The charge and spin figure of merits as functions of the dot level and the temperature for $\Delta = 0.3\Gamma_0$. Other parameters are as in Fig. 2

in Fig. 4b is smaller as compared to the charge one. This is because that with increasing temperature, the interference effect becomes less distinct and the spin thermoelectric effect is drastically affected. Moreover, in higher temperature the thermopower approaches to zero, resulting in reduced FOMs.

Figure 5 shows the dependence of the thermopwers and the FOMs on the dot level ε_0 for fixed $\Delta = 0.5\Gamma_0$, $P_R = 0.4$ and different values of P_L. The magnitude of the charge thermopower S_c in Fig. 5a is monotonously enhanced by increasing P_L. This is because that the assumption of the spin dependence resulting from the line-width functions is essentially equivalent to the spin-dependent density of states at the Fermi level. Increased P_L denotes sharper change of the electron density of states and then enhances the thermoelectric effect in nanostructures as mentioned above. The enhancement of the spin thermopower S_s in Fig. 5b is more obvious than the the case of charge one as compared to the inset in Fig. 5a. This is because that the spin effects of the devices is more distinct with the increase of the spin polarization of the leads. The magnitude of the charge FOM in Fig. 5c is also

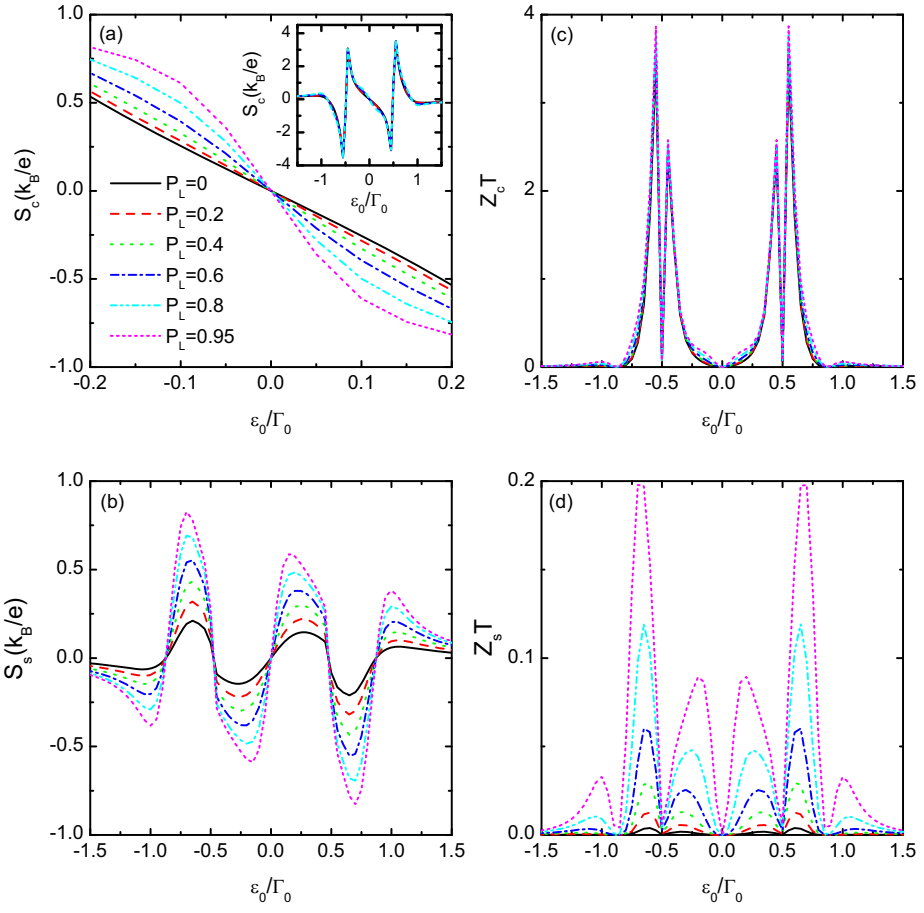

Fig. 5 **a** Charge Seebeck coefficient, **b** spin Seebeck coefficient, **c** charge figure of merit, and **d** spin figure of merit as functions of the dot level for different spin polarizations of the left lead P_L with fixed $P_R = 0.4$ and $\Delta = 0.5\Gamma_0$. Other parameters are as in Fig. 2

monotonously enhanced with increasing P_L with unchanged line-shape. The spin FOM Z_sT in Fig. 5d is also obviously enhanced as compared to Z_cT for increasing P_L with increased peaks' width. The magnitude of the maximum Z_sT is still one order of smaller than that of the charge one.

Now we see that the enhancement of the spin thermoelectric signals by the ferromagnetic leads is rather limited, and then we turn to study the effects of the spin-dependent interdot coupling. As seen from Fig. 6a and b, the peaks' values of the charge thermopower S_c are suppressed by increasing δt_c. Such a situation is independent of the signs of δt_c. The reason can be explained as follows: The function of $t_{ij,\sigma}$ is mainly to change the position of the resonant and anti-resonant states, which induces peaks in the thermopower. In the presence of δt_c, the spin-up and spin-down anti-resonant states, which locate at the same positions for $\delta t_c = 0$, are separated away. As a result of it, the peak value of the charge thermopower at each anti-resonant state is only determined by the spin-up electrons. Such an effect is strengthened by the ferromagnetic leads arranged in parallel configuration. For $\delta t_c = 0.5\Gamma_0$ as shown by the blue dash-dot line in Fig. 6a, the contribution of spin-down electrons to S_c is totally suppressed as $t_{ij,\downarrow} = 0$, resulting in minimum S_c. For $\delta t_c < 0$ in Fig. 6b, the behavior of S_c can be explained in the same way. It is noted that two small peaks at the two sides of $\varepsilon_0 = 0$ emerge due to the shift of the anti-resonant states of spin-up and spin-down components. The above explanations are confirmed by the behaviors of the spin thermopower S_s in Fig. 6c for $\delta t_c > 0$. Now the contribution of the spin-up electrons to the thermoelectric transport is predominant and then the value of $S_c = S_\uparrow - S_\downarrow$ is positive. Since the value of $S_\downarrow$ is reduced by increasing δt_c, the magnitude of S_s is enhanced accordingly.

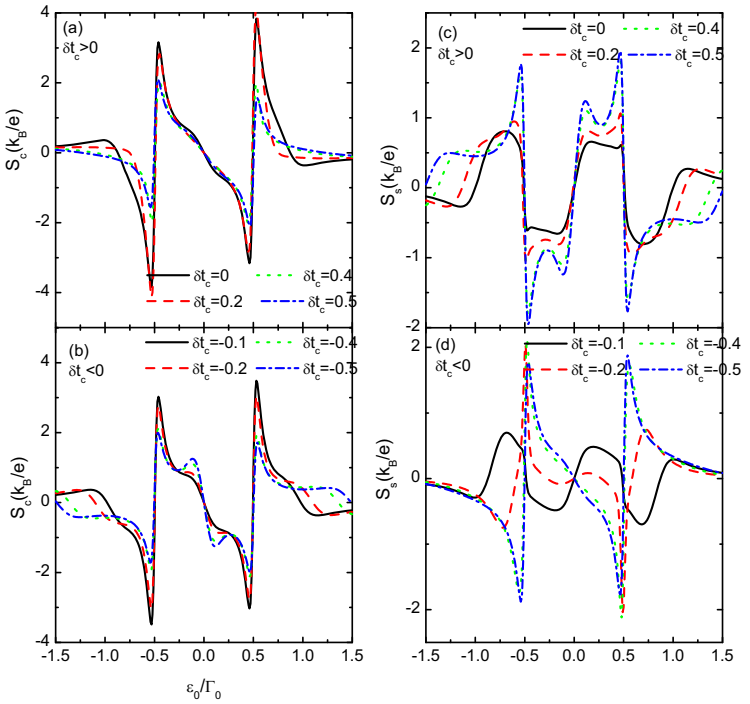

Fig. 6 **a**, **b** Charge Seebeck coefficients, and **c**, **d** spin Seebeck coefficients as functions of the dot level for different δt_c for $P_L = 0.8$, $P_R = 0.4$ and $\Delta = 0.5\Gamma_0$. Other parameters are as in Fig. 2

For $\delta t_c = 0.5\Gamma_0$ (the dash-dot blue line), the magnitude of S_s equals to that of the charge thermopower S_c. As for $\delta t_c < 0$, the spin thermopower changes its sign as now the majority spin in the two leads is spin-up due to the presence of the magnetic leads arranged in parallel configuration.

The charge thermopower in Fig. 7a and b can be either enhanced or reduced by changing the value and the sign of δt_c. Similar to the case of the thermopower in Fig. 6b, Z_cT also has two small peaks at the two sides of $\varepsilon_0 = 0$. The magnitude of Z_cT may increase for $\delta t_c > 0$ as shown in Fig. 7a. But under the condition of $\delta t_c < 0$ in Fig. 7b, Z_cT is monotonously reduced with increasing absolute value of δt_c. The changes of Z_sT in Fig. 7c and d are opposite to the Z_cT. Especially for $\delta t_c < 0$, the magnitudes of the charge and spin FOMs are individually reduced and enhanced.

In Fig. 8 we present the thermoelectric quantities as functions of ε_0 for different values of $U_1 = U_2 = U_3 = U$. Due to the Coulomb blockade effect, the cures in the electric conductance and the thermal conductivity develop new peaks located at $\varepsilon_0 = \mu$ and $\varepsilon_0 = \mu - U$ [56, 57]. Moreover, besides the four anti-resonant points induced by the quantum destructive interference, a new zero point at G_σ appears at the electron hole symmetry point $\varepsilon_0 = -U/2$, which also induces peaks in the thermopower as seen from Fig. 8a. At the resonant points and zero points of G_σ, the electron contributions to the current are compensated by the holes and the charge thermopower is zero and changes sign when the dot level is aligned to these states [Fig. 8a]. The charge FOM is presented in Fig. 8b, which is mainly dominated by five double-peak structures. Four double peaks are near the anti-resonant points, and one is near the electron hole symmetry point. For small intradot U, the spectral line induced by the quantum interference effect overlaps with that by the Coulomb interaction and results in

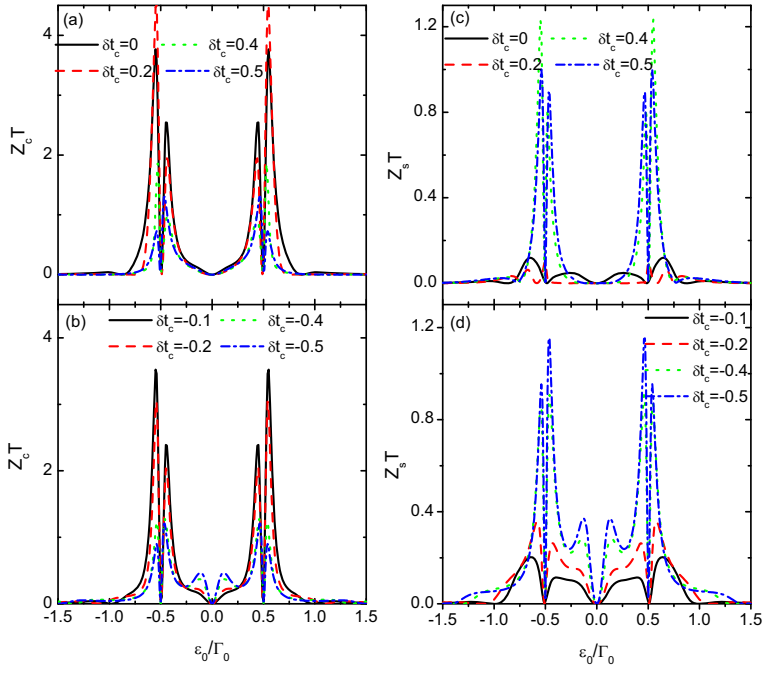

Fig. 7 **a**, **b** Charge figure of merit, and **c**, **d** spin figure of merit as functions of the dot level for different δt_c. Parameters are as in Figs. 2 and 6

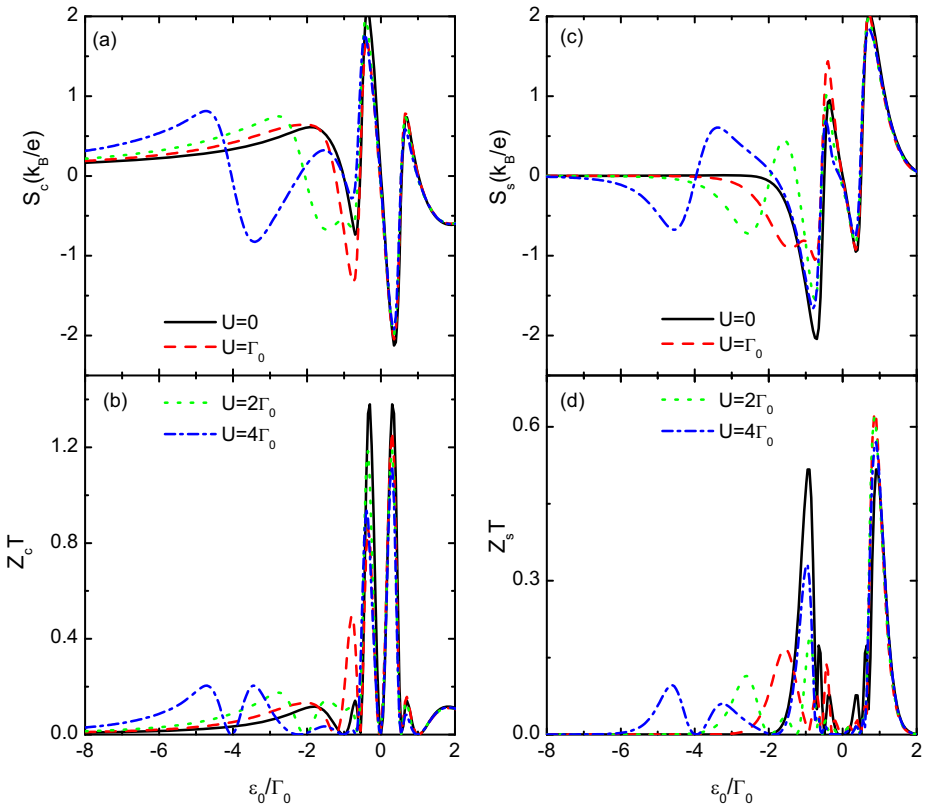

Fig. 8 **a** Charge Seebeck coefficient, **b** Charge figure of merit, **c** spin Seebeck coefficient, and **d** spin figure of merit as functions of the dot level for different intradot Coulomb interaction U. The adopted parameters are $k_BT = 0.1\Gamma_0$, $t_c = 0.5\Gamma_0$, $\Delta = 0.5\Gamma_0$, $p_L = 0.8$, $p_R = 0.4$ and $\delta t_c = 0.4\Gamma_0$

complex structures of S_c and Z_cT, whose magnitudes may be enhanced by incorporation of the adjacent peaks. The spin thermopower S_s in Fig. 8c develop peaks at the same points to the charge counterpart, but the sign is reversed. For large intradot Coulomb, the magnitude S_s is obviously enhanced, as shown by the green dot and blue dash-dot lines. The structure of the spin FOM Z_sT in Fig. 8d also resembles that of the charge one Z_cT in Fig. 8b. It can be seen that the magnitude of Z_sT can be either strengthened or suppressed at some particular states by changing the intradot Coulomb interaction. For example, at $\varepsilon_0 = -\Gamma_0$, the value of Z_sT is monotonously reduced by increasing U, whereas at $\varepsilon_0 = \Gamma_0$ Z_sT it is enhanced. Such a phenomenon can be attributed to the overlap of the resonant and anti-resonant states induced by quantum interference and Coulomb blockade effects.

4 Conclusion

Spin seebeck effect is studied in a triple QDs ring connected to ferromagnetic leads with spin-dependent interdot couplings. It is found that the magnitude of the thermoelectric quantities including spin thermopower and spin FOM are obviously enhanced by the quantum destructive interference effect due to the ring shape of the structure. The joint effect of the

ferromagnetism on the leads and the spin-dependent interdot couplings result in large spin thermopower and spin FOM, whose magnitude may reach as high as those of the charge counterparts. Moreover, the sign of the spin thermoepower can also be changed by changing the magnetic moments of the leads and the spin-dependent interdot couplings.

Acknowledgments This work is supported by the NSFC (Grant Nos. 61274101 and 51362031), and the Initial Project of UEST of China, Zhongshan Institute (415YKQ02). This work is also supported by the Innovation Team of Zhongshan City (No. 170615151170710).

References

1. Giazotto, F., Heikkila, T.T., Luukanen, A., Savin, A.M., Pekola, J.P.: Rev. Mod. Phys **78**, 217 (2006)
2. Dubi, Y., Di Ventra, M.: Rev. Mod. Phys **83**, 131 (2011)
3. Kubala, B., Konig, J., Pekola, J.: Phys. Rev. Lett. **100**, 066801 (2008)
4. Garg, A., Rasch, D., Shimshoni, E., Rosch, A.: Phys. Rev. Lett. **103**, 096402 (2009)
5. Wolf, S.A., Awschalom, D.D., Buhrman, R.A., Daughton, J.M., von Molnar, S., Roukes, M.L., Chtchelkanova, A.Y., Treger, D.M.: Science **294**, 1488 (2001)
6. Zutic, I., Fabian, J., Sarma, S.D.: Rev. Mod. Phys **76**, 323 (2004)
7. Bauer, G.E.W., Saitoh, E., van Wees, B.J.: Nat. Mater **11**, 391 (2012)
8. Uchida, K., Takahashi, S., Harii, K., Ieda, J., Koshibae, W., Ando, K., Maekawa, S., Saitoh, E.: Nature (London) **455**, 778 (2008)
9. Jaworski, C.M., Yang, J., Mack, S., Awschalom, D.D., Heremans, J.P., Myers, R.C.: Nat. Mater **9**, 898 (2010)
10. Qu, D., Huang, S.Y., Hu, J., Wu, R., Chien, C.L.: Phys. Rev. Lett. **110**, 067206 (2013)
11. Uchida, K., Xiao, J., Adachi, H., Ohe, J., Takahashi, S., Ieda, J., Ota, T., Kajiwara, Y., Umezawa, H., Kawai, H., Bauer, G.E.W., Maekawa, S., Saitoh, E.: Nat. Mater **9**, 894 (2010)
12. Uchida, K., Adachi, H., Ota, T., Nakayama, H., Maekawa, S., Saitoh, E.: Appl. Phys. Lett. **97**, 172505 (2010)
13. Kajiwara, Y., Harii, K., Takahashi, S., Ohe, J., Uchida, K., Mizuguchi, M., Umezawa, H., Kawai, H., Ando, K., Takanashi, K., Maekawa, S., Saitoh, E.: Nature (London) **464**, 262 (2010)
14. Yu, H., Granville, S., Yu, D.P., Ansermet, J.P.: Phys. Rev. Lett. **104**, 146601 (2010)
15. Dyrdal, A., Barnaś, J.: J. Nanosci. Nanotechnol. **12**, 9051 (2012)
16. Kirihara, A., Uchida, K., Kajiwara, Y., Ishida, M., Nakamura, Y., Manako, T., Saitoh, E., Yorozu, S.: Nat. Mater **11**, 686 (2012)
17. Zhang, L., Ren, J., Wang, J.-S., Li, B.: Phys. Rev. B **87**, 144101 (2013)
18. Zhang, Z.H., Bai, L.H., Chen, X.B., Guo, H., Fan, X.L., Xue, D.S., Houssameddine, D., Hu, C.M.: Phys. Rev. B **94**, 064414 (2016)
19. Alekhin, A., Razdolski, I., Ilin, N., Meyburg, J.P., Diesing, D., Roddatis, V., Rungger, I., Stamenova, M., Sanvito, S., Bovensiepen, U., Melnikov, A.: Phys. Rev. Lett. **119**, 017202 (2017)
20. Okuma, N., Masir, M.R., MacDonald, A.H.: Phys. Rev. B **95**, 165418 (2017)
21. Uchida, K., Iguchi, R., Daimon, S., Ramos, R., Anadon, A., Lucas, I., Algarabel, P.A., Morellon, L., Aguirre, M.H., Ibarra, M.R., Saitoh, E.: Phys. Rev. B **95**, 184437 (2017)
22. Wu, B.W., Luo, G.Y., Lin, J.G., Huang, S.Y.: Phys. Rev. B **96**, 060402(R) (2017)
23. Ohnuma, Y., Matsuo, M., Maekawa, S.: Phys. Rev. B **96**, 134412 (2017)
24. Giles, B.L., Yang, Z.H., Jamison, J.S., Gomez-Perez, J.M., Vélez, S., Hueso, L.E., Casanova, F., Myers, R.C.: Phys. Rev. B **96**, 180412(R) (2017)
25. van der Wiel, W.G., Franceschi, S. De., Elzerman, J.M., Fujisawa, T., Tarucha, S., Kouwenhoven, L.P.: Rev. Mod. Phys **75**, 1 (2003)
26. Wang, Z.M.: Self-Assembled Quantum Dots. Springer, New York (2008)
27. Dubi, Y., Ventra, M.D.: Phys. Rev. B **79**, 018302(R) (2009)
28. Ramos-Andrade, J.P., Peña, F.J., González, A., Àvalos-Ovando, O., Orellana, P.A.: Phys. Rev. B **96**, 165413 (2017)
29. Liu, Y.S., Chi, F., Yang, X.F., Feng, J.F.: J. Appl. Phys. **109**, 053712 (2011)
30. Silva, G.G., Ovando, O., Guevara, M.L.L., Orellana, P.A.: Phys. E (Amsterdam Neth.) **63**, 311 (2014)
31. Jiang, F., Shi, C., Yan, Y., Xie, H., Yan, Y.: Phys. Lett. A **379**, 435 (2015)
32. Liu, Y.S., Yang, X.F., Chi, F., Si, M.S., Guo, Y.: Appl. Phys. Lett. **101**, 213109 (2012)
33. Krawiec, M., Wysokinski, K.I.: Phys. Rev. B **73**, 075307 (2006)

34. Świrkowicz, R., Wierzbicki, M., Barnaś, J.: Phys. Rev. B **80**, 195409 (2009)
35. Wierzbicki, M., Świrkowicz, R.: Phys. Rev. B **82**, 165334 (2010)
36. Chen, X.B., Liu, D.P., Duan, W.H., Guo, H.: Phys. Rev. B **87**, 085427 (2013)
37. Wójcik, K.P., Weymann, I.: Phys. Rev. B **93**, 085428 (2016)
38. Karwacki, L., Trocha, P.: Phys. Rev. B **94**, 085418 (2016)
39. López, R., Lee, M., Serra, L., Lim, J.S.: Phys. Rev. B **89**, 205418 (2014)
40. Hwang, S.Y., Sánchez, D., López, R.: New J. Phys. **18**, 093024 (2016)
41. Weymann, I.: J. Phys.: Condens. Matter **29**, 095301 (2017)
42. Kolenda, S., Sürgers, C., Fischer, G., Beckmann, D.: Phys. Rev. B **95**, 224505 (2017)
43. Ladrón de Guevara, M.L., Claro, F., Orellana1, P.A.: Phys. Rev. B **67**, 195335 (2003)
44. Wang, Q., Xie, H.Q., Nie, Y.H., Ren, W.: Phys. Rev. B **87**, 075102 (2013)
45. Noiri, A., Takakura, T., Obata, T., Otsuka, T., Nakajima, T., Yoneda, J., Tarucha, S.: Phys. Rev. B **96**, 155414 (2017)
46. Niklas, M., Trottmann, A., Donarini, A., Grifoni, M.: Phys. Rev. B **95**, 115133 (2017)
47. Büttiker, M.: Phys. Rev. B **27**, 6178 (1983)
48. Hüttel, A.K., Ludwig, S., Lorenz, H., Eberl, K., Kotthaus, J.P.: Phys. Rev. B **72**, 081310(R) (2005)
49. Zhang, P., Xue, Q.K., Wang, Y.P., Xie, X.C.: Phys. Rev. Lett. **89**, 286803 (2002)
50. Li, Z.J., Jin, Y.H., Nie, Y.H., Liang, J.Q.: J. Phys.: Condens. Matter **20**, 085214 (2008)
51. Wang, H.X., Yin, W., Wang, F.W.: J. Appl. Phys. **109**, 053710 (2011)
52. Sun, Q.F., Xie, X.C.: Phys. Rev. B. **73**, 235302 (2006)
53. Sun, Q.F., Xing, Y.X., Shen, S.Q.: Phys. Rev. B. **77**, 195313 (2008)
54. Beenakker, C.W.J., Staring, A.A.M.: Phys. Rev. B **46**, 9667 (1992)
55. Chi, F., Zheng, J., Liu, Y.S., Guo, Y.: Appl. Phys. Lett. **100**, 233106 (2012)
56. Liu, J., Sun, Q.F., Xie, X.C.: Phys. Rev. B **81**, 245323 (2010)
57. Chi, F., Zheng, J., Lu, X.D., Zhang, K.C.: Phys. Lett. A **375**, 1352 (2011)